

# TRANSCRITICAL AND HOPF BIFURCATIONS IN AC/DC SYSTEMS

**Claudio A. Cañizares**      **Steve Hranilovic**  
 University of Waterloo  
 Department of Electrical & Computer Engineering  
 Waterloo, ON, Canada    N2L 3G1

**Abstract:** This paper illustrates transcritical and Hopf bifurcations in a realistic ac/dc power system model. These bifurcations are thoroughly analyzed based on bifurcation theory to understand and characterize their effect on the dynamic behavior of the system, particularly on voltage stability. A new technique to trace transcritical bifurcations diagrams is proposed, based on the generic characteristic of saddle-node bifurcations for constant P load changes, as demonstrated in the paper. Control mechanisms for avoiding the bifurcations are also presented. Finally, the paper discusses the computational requirements for studying possible chaotic behavior due to bifurcations on the system limit cycles.

**Keywords:** transcritical bifurcations, Hopf bifurcations, generic saddle-node bifurcations, chaos, voltage stability and control.

## 1. Introduction

Hopf and saddle-node bifurcations have been recognized as some of the reasons, albeit not the only ones, for stability problems in a variety of power system models [2]–[13]. These local bifurcations are detected by monitoring the eigenvalues of the current operating point. As certain parameters in the system change slowly, allowing the system to quickly recover and maintain a stable operating point, the system eventually turns unstable, either due to one of the eigenvalues becoming zero (saddle-node, transcritical, pitchfork bifurcations), or due to a pair of complex conjugate eigenvalues crossing the imaginary axes of the complex plane (Hopf bifurcation). The instability of the system is reflected on the state variables, i.e., frequency, angles, voltages and currents, by an oscillatory behavior or a continuous change that lead to voltage collapse *and* loss of synchronism. In some cases saddle-node bifurcations can be associated to the power transfer limit of the transmission system [6]; in other instances Hopf bifurcations appear due to voltage control problems, such as fast acting automatic voltage regulators (AVR) in the generators [12]. In all cases these bifurcations occur on very stressed systems, i.e., the region of stability for the current operating point (stable equilibrium point or s.e.p.) is small [6, 14], hence, the system is not able to withstand small perturbations and becomes unstable. Although there are reports of these bifurcations occurring in unstressed systems [13], this cannot be considered typical, since power system controls are designed so that eigenvalues of various operating points are well into the left half complex plane.

Some voltage collapse problems are not directly associated to bifurcations, but are generated by voltage control devices such as under-load tap changers (ULTCs) or AVRs [15]–[18]. In some of these cases the voltage controls force the eigenvalues to instantaneously jump into the unstable region, making

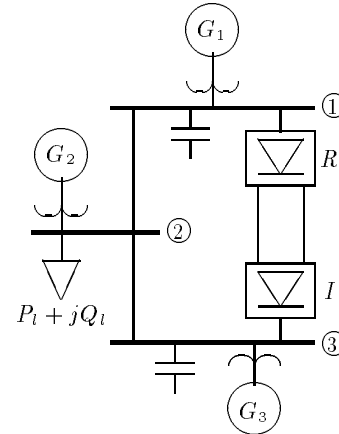


Fig. 1: Sample ac/dc system

the system immediately unstable. Although this particular phenomena is not directly associated to a bifurcation, since the eigenvalues do not go through zero or the imaginary axis, transcritical bifurcation theory can be used to explain the phenomena when AVR limits are assumed to apply gradually [16].

Hopf bifurcations have been detected in a variety of power system models [7, 11, 12, 13]. Particularly, in reference [11] a thorough study of this problem and period doubling bifurcations is presented for a simple dynamic model of 4 state variables and no algebraic constraints. On the other hand, there is little reference in the literature to transcritical bifurcations in typical power system models. This can be explained based on the fact that these types of bifurcations, as formally shown in this paper, are not generic and they only occur under certain assumptions that give the problem a special symmetry [19, 20].

This paper focuses on studying transcritical and Hopf bifurcations in a realistic model of the ac/dc system depicted in Fig. 1, with two different sets of data and system parameters to obtain the desired bifurcations. This network can be represented by a set of differential and algebraic equations [7, 21]. For each case, time simulations and eigenvalue analyses are carried out to study and depict the phenomena, and based on the results, control mechanisms are implemented to try to avoid the stability problems generated by these bifurcations. The paper also discusses the computational requirements and techniques needed for studying these bifurcations. Particularly, the last section is dedicated to discuss the problems of implementing known techniques to study bifurcations on limit cycles that lead to chaotic behavior.

## 2. Transcritical Bifurcations

The system model of references [7, 21] is used. This is a typical dynamic model useful for transient and voltage stability studies. Thus, a second order synchronous generator model is used, with constant terminal voltage, reactive power limits, and constant mechanical power that changes with system load level; this simulates some of the effects of the AVR and the governor. A  $\Pi$ -equivalent circuit model is employed to represent all the elements of the transmission system; transformers and phase shifters are included as part of this transmission network. A ZIP load model with dynamic voltage and frequency dependent terms is used, since this simulates a wide variety of aggregated power system loads. It is important to mention that the location of the bifurcations depend significantly on the static load models used, as demonstrated in reference [6].

DC lines are simulated using R-L circuits, and HVDC controllers are modeled using saturable PI current controllers with  $K_P$  (Proportional) and  $K_I$  (Integral) gains. Although these control circuits are only approximations to the more complicated HVDC control structures, they recreate several of the main properties of the actual control systems, especially when close to the equilibria. Power controls and Voltage Dependent Current Order Limiters (VDCOL) are introduced into this model by representing the controller current order as a function of the converter voltages.

This system model can be summarized in the following set of equations [7, 21]:

$$\begin{cases} \dot{\mathbf{x}} = \mathbf{f}(\mathbf{x}, \mathbf{y}, \lambda) \\ \mathbf{0} = \mathbf{g}(\mathbf{x}, \mathbf{y}, \lambda) \end{cases} \Rightarrow \begin{bmatrix} \dot{\mathbf{x}} \\ \mathbf{0} \end{bmatrix} = \mathbf{F}(\mathbf{z}, \lambda) \quad (1)$$

where  $\mathbf{x} \in \mathbb{R}^n$  is a vector of state variables,  $\mathbf{y} \in \mathbb{R}^m$  is a vector of algebraic variables,  $\mathbf{z} \triangleq [\mathbf{x}^T \ \mathbf{y}^T]^T$ , and  $\lambda \in \mathbb{R}$  is any parameter in the system that changes slowly, moving the system from one s.e.p. to another until a bifurcation is encountered. For this one-parameter dynamical system, non-singularity of the Jacobian  $D_y \mathbf{g}(\cdot)$  along system trajectories of interest, guarantees a well posed system [22] or strictly causal system [4], i.e., for these trajectories

$$\begin{aligned} \mathbf{y} &\triangleq \mathbf{h}(\mathbf{x}) \\ \mathbf{s}(\mathbf{x}, \lambda) &\triangleq \mathbf{f}(\mathbf{x}, \mathbf{h}(\mathbf{x}), \lambda) \\ \Rightarrow \dot{\mathbf{x}} &= \mathbf{s}(\mathbf{x}, \lambda) \end{aligned} \quad (2)$$

If  $D_y \mathbf{g}(\cdot)$  becomes singular, then the model represented by equations (1) breaks down. When this occurs, dynamic load models may be introduced to transform some algebraic constraints into differential equations to remove the singularity, which is similar to the singular perturbation approach proposed in [22].

For this particular model, bifurcations characterized by a singular dynamic Jacobian  $D_x \mathbf{s}|_0$  at the equilibrium point  $(\mathbf{x}_0, \mathbf{y}_0, \lambda_0)$  with nonsingular  $D_y \mathbf{g}|_0$ , can be detected using either the Jacobian of the full steady state equations  $\mathbf{F}(\cdot) \triangleq [\mathbf{f}^T(\cdot) \ \mathbf{g}^T(\cdot)]^T = \mathbf{0}$ , or the Jacobian of the power flow equations, which are a subset of the steady state equations including detailed static load models, as thoroughly demonstrated in reference [21]. Of these particular local bifurcations only saddle-nodes are generic [19, 20], i.e., they are expected

to take place under typical operating conditions and modeling assumptions. However, transcritical and pitchfork bifurcations could also occur when the system presents a special symmetry due to certain modeling assumptions [19, 20], as shown below for an ac/dc test system.

### 2.1. Background

The following conditions apply for a transcritical bifurcation of equations (1) at the equilibrium point  $(\mathbf{x}_0, \mathbf{y}_0, \lambda_0)$  where  $D_y \mathbf{g}|_0$  is non-singular [19]:

$$1. \ D_x \mathbf{s}|_0 \triangleq D_x \mathbf{s}(\mathbf{x}_0, \lambda_0) \text{ has a simple and unique zero eigenvalue, with normalized right eigenvector } \mathbf{v} \text{ and left eigenvector } \mathbf{w}, \text{ i.e., } D_x \mathbf{s}|_0 \mathbf{v} = \mathbf{0} \text{ and } \mathbf{w}^T D_x \mathbf{s}|_0 = \mathbf{0}^T \quad (3)$$

$$2. \ \mathbf{w}^T \frac{\partial \mathbf{s}}{\partial \lambda} \Big|_0 = 0, \text{ and } \mathbf{w}^T D_{\lambda_x}^2 \mathbf{s}|_0 \mathbf{v} \neq 0 \quad (4)$$

$$3. \ \mathbf{w}^T [D_x^2 \mathbf{s}|_0 \mathbf{v}] \neq 0 \quad (5)$$

Observe that from (1) and (2),

$$D_x \mathbf{s}|_0 = D_x \mathbf{f}|_0 - D_y \mathbf{f}|_0 D_y \mathbf{g}|_0^{-1} D_x \mathbf{g}|_0$$

Hence, these conditions have an equivalent representation for the steady state and power flow equations [21], i.e.,

$$1. \ D_z \mathbf{F}|_0 \triangleq D_z \mathbf{F}(\mathbf{z}_0, \lambda_0) \text{ has a zero eigenvalue, with unique normalized right eigenvector } v \text{ and left eigenvector } \omega, \text{ i.e., } D_z \mathbf{F}|_0 v = \mathbf{0} \text{ and } \omega^T D_z \mathbf{F}|_0 = \mathbf{0}^T \quad (6)$$

$$2. \ \omega^T \frac{\partial \mathbf{F}}{\partial \lambda} \Big|_0 = 0 \quad (7)$$

$$3. \ \omega^T [D_z^2 \mathbf{F}|_0 v] \neq 0 \quad (8)$$

Observe that in general,  $\mathbf{w}^T D_{\lambda_x}^2 \mathbf{s}|_0 \mathbf{v} \neq \omega^T D_{\lambda_z}^2 \mathbf{F}|_0 v$ .

Parameterized continuation and direct methods can be used to trace the bifurcation diagrams and determine the exact location of these bifurcations, respectively [18, 20]. Furthermore, conditions (3), (4) and (5) can be used to prove that these methods have nonsingular Jacobians of the associated equations at the bifurcation point, by following similar steps to the ones used for saddle-node bifurcations in references [21, 23].

Continuation methods run into problems when constructing transcritical bifurcations diagrams, because in this case, as opposed to saddle-node bifurcations, there are two independent paths of equilibria to be traced, which cross transversally at the bifurcation point. Tracing one branch with this method gives the approximate location of the bifurcation point; however, it does not yield much information with regards to the location of the second path of equilibrium points. To find the direction that the second branch follows, researchers have developed techniques aimed at finding the tangent vectors of the two branches at the bifurcation point, which is a nontrivial problem [20]. Another approach is to find a point on the second branch of equilibria for certain value of the parameter  $\lambda$ , using then this point to apply the continuation method to trace the corresponding branch; this is done by finding an approximation of a perpendicular vector to one of the branches near the bifurcation [20]. Although the latter is computationally more efficient, it also presents several difficulties.

This paper presents a different and novel solution to the problem of tracing the second branch of equilibria in power

systems. The idea is also to find a point on the second branch for a fixed value of  $\lambda$ , but relying in this case on the generic characteristic of saddle-nodes for certain parameters in the system. Thus, for a particular operating point, i.e., for a given value of  $\lambda$ , one chooses a constant P load as the new system parameter, so that the system bifurcates through a saddle-node instead of a transcritical bifurcation, as demonstrated below. Hence, the saddle-node bifurcation diagram can now be fully traced around the bifurcation to find the desired point on the second branch for the chosen operating conditions.

To show that the saddle-node is a generic bifurcation when a constant P load change is chosen as the new system parameter, one starts by observing that for this particular choice of  $\lambda$  and for the system model described in [21, 23],

$$\frac{\partial \mathbf{s}}{\partial \lambda}(\mathbf{x}, \lambda) = \mathbf{k} \quad \forall \mathbf{x} \in \mathfrak{R}^n, \lambda \in \mathfrak{R}$$

where  $\mathbf{k} \in \mathfrak{R}^n$  is a constant vector and  $\lambda$  represents the new load parameter. Hence, the second transversality condition (4) required in transcritical and pitchfork bifurcations [19], is not met since

$$D_{\lambda x}^2 \mathbf{s}(\mathbf{x}, \lambda) = \mathbf{0} \quad \forall \mathbf{x} \in \mathfrak{R}^n, \lambda \in \mathfrak{R}$$

Thus, the local bifurcation associated to a singular eigenvalue in this system is a saddle-node, which is characterized by transversality conditions (3), (5), and

$$\mathbf{w}^T \frac{\partial \mathbf{s}}{\partial \lambda} \Big|_0 = \mathbf{w}^T \mathbf{k} \neq 0$$

## 2.2. Example

The data in Tables 1, 2 and 3 are used in the ac/dc test system of Fig. 1 to obtain a transcritical bifurcation. In this case, the impedance of transformer  $G_3$  at the inverter side is used as the system parameter  $\lambda$ , so that the effect of Short Circuit Ratio (SCR) changes in the overall ac/dc system can be studied. Generator  $G_3$  is modeled using a large inertia and damping, as shown in Table 2, to represent a large system on the inverter side. Moreover, this generator keeps  $V_3$  at 1p.u. when the SCR changes by using an open-loop control strategy, which is not a typical approach to remote voltage control; this particular modeling assumption yields the transcritical bifurcation, as shown below. The generator  $G_2$  is modeled as a constant power source supplying the local load demand of  $P_l = 0.1$ p.u. and  $Q_l = 0$ , and has no bearing in the dynamic behavior of the system for the transcritical bifurcation study. These generator and load at bus 2 are only used to transform the problem from a transcritical into a saddle-node bifurcation, by making  $P_l$  the new system parameter for a given value of the inverter SCR, so that the second branch of equilibria can be traced using the technique described above. Observe in Table 1 that the ac link between rectifier and inverter is very weak, so that ac voltage changes in one converter do not affect the other through the ac transmission system, which is the typical situation in long HVDC links. Finally, the HVDC is assumed to operate under power control in the rectifier and extinction angle control in the inverter, within the angle limits depicted in Table 3.

All the results depicted in this paper were obtained using a variety of tools and simulation packages, namely, PFLOW [18], SOLVER-Q [24], EES [25], MATLAB [26], and MAPLEV [27].

Element	$G$	$B$	$-B_s$
Line 1-2	0	1.1513	0
Line 2-3	0	1.1513	0
Transf. $G_1$	0	146.63	0
Transf. $G_2$	0	100.00	0
Transf. $G_3$	0	$\lambda$	0
Capac. 1	0	0	13.75
Capac. 3	0	0	21.46

**Table 1:** AC transmission system data in p.u. for a 230 kV and 100 MVA base.

Variable	$G_1$	$G_2$	$G_3$
Inertia $M$	$\infty$	—	1
Damping $D$	—	—	1
Terminal Voltage $V_t$	1.05	—	—
Mechanical Power $P_m$	—	0.1	27.72

**Table 2:** Generator data in p.u. for a 13.8 kV and 100 MVA base

Figure 2 shows the bifurcation diagram for both ac converter voltages  $V_1$  and  $V_3$  as the inverter SCR changes. The eigenvalues were calculated for all system equilibria; thus, the s.e.p.s are depicted in this figure with continuous lines, whereas the unstable equilibrium points (u.e.p.s) are represented by dashed lines. These curves were traced using a continuation method with the branch switching technique described above. Notice the characteristic  $\times$  crossing at the bifurcation point, where the s.e.p. associated to  $V_3 = 1$ p.u. changes into a u.e.p. Figure 3 depicts, for both equilibria branches, the real part of the eigenvalues of  $D_x \mathbf{s}|_0$  closest to the imaginary axis, showing how this matrix becomes singular at SCR=2.2123.

The exact bifurcation point was calculated applying a direct method to the full set of steady state equations  $\mathbf{F}(\mathbf{z}, \lambda) = \mathbf{0}$ , since the symbolic Jacobian  $D_z \mathbf{F}(\mathbf{z}, \lambda)$  can be easily computed. This method cannot be applied in practice to the symbolic transient Jacobian  $D_x \mathbf{s}(\mathbf{x}, \lambda)$ , since this matrix is difficult to obtain symbolically (it takes several days using MAPLEV in a 32MB-RAM SPARCSTATION-LX with 200MB swap space). On the other hand, using numerical approximations to  $D_x \mathbf{s}(\cdot)$  significantly affect the convergence characteristics of the nu-

Variable	Rectifier	Inverter
$K_P$	1	1
$K_I$	43.5	43.5
Commutation reactance $X_c$	0.06654	0.06541
Tap $a$	3.7077	3.3731
Min. firing angle $\alpha_{min}$	$5^\circ$	$\sim 120^{0\dagger}$
Max. firing angle $\alpha_{max}$	$120^\circ$	$\sim 142^{0\dagger}$
Min. extinction angle $\gamma_{min}$	$\sim 40^{0\dagger}$	$18^\circ$
Max. extinction angle $\gamma_{max}$	$\sim 155^{0\dagger}$	$40^\circ$
Power order $P_r$	31.42	—
Extinction angle order $\gamma_i$	—	$18^\circ$
DC resistance $R_d$	0.072892	
DC inductance $L_d$	0.008695	

$\dagger$  Assuming  $\mu \approx 20^\circ$

**Table 3:** DC system data in p.u. for a 230 kV and 435 A base.

merical techniques used to solve the direct method equations.

Time domain simulations were carried out to study the effects of changing the SCR from a pre-bifurcation value to a post-bifurcation one, and see whether the system becomes unstable or recovers to a new equilibrium point on the second branch. The results of these simulations are shown in Figs. 4 and 5. In Fig. 4 the generator  $G_3$  terminal voltage  $V_{t_{G_3}}$  is changed after 0.5sec. to keep  $V_3$  at 1p.u. In this case the system becomes unstable, with a clear voltage collapse of the inverter ac voltage and large changes in generator frequency and HVDC variables. Observe that some of the system variables oscillate in a stable limit cycle, which could be attributed to the HVDC controls. If  $V_{t_{G_3}}$  is instantaneously changed, the system recovers and converges to the stable equilibrium point on the second branch of the transcritical bifurcation diagram, as shown in Fig. 5.

The results from the simulation demonstrate the importance of controlling the inverter ac voltage. Hence, a fast closed-loop control is introduced in the system to maintain  $V_3$  at 1p.u. by instantaneously changing  $V_{t_{G_3}}$ , i.e.,  $V_3 = 1$ p.u. for all system simulations. This is a more realistic control strategy than the open-loop control approach, and it eliminates the special symmetry responsible for the transcritical bifurcation, making all system equilibria stable for any value of SCR. Nevertheless, limits, gains, and time delays should be included for a more accurate representation of this type of remote voltage control.

### 3. Hopf Bifurcations

Hopf bifurcations are also generic bifurcations of dynamic systems represented by equations (2) [19, 20]. These types of bifurcations can be shown not to exist in a simple lossless power system model [28]; however, they have been observed in a variety of more realistic power system models [7, 11, 12, 13]. The following sections concentrate on discussing the theory of Hopf bifurcations and the methods used to study them, highlighting their computational requirements and limitations when applied to the ac/dc test system of Fig. 1.

#### 3.1. Background

The transversality conditions of a Hopf bifurcation for equations (1) at the equilibrium point  $(\mathbf{x}_0, \mathbf{y}_0, \lambda_0)$ , where  $D_{\mathbf{y}}\mathbf{g}|_0$  is non-singular, are [19, 20]:

1.  $D_x \mathbf{s}|_0$  has a simple pair of purely imaginary eigenvalues

$$\mu(\lambda_0) = \pm j\beta \quad (9)$$

and no other eigenvalue with zero real part.

2. These eigenvalues cross the imaginary axis with “non-zero speed”, i.e.,

$$\frac{d\text{Re}\{\mu(\lambda_0)\}}{d\lambda} \neq 0 \quad (10)$$

This bifurcation gives birth to a zero-amplitude oscillation (limit cycle) with initial period

$$T_0 = \frac{2\pi}{\beta}$$

Hopf bifurcations can be detected using a continuation method to trace the system equilibria while monitoring the

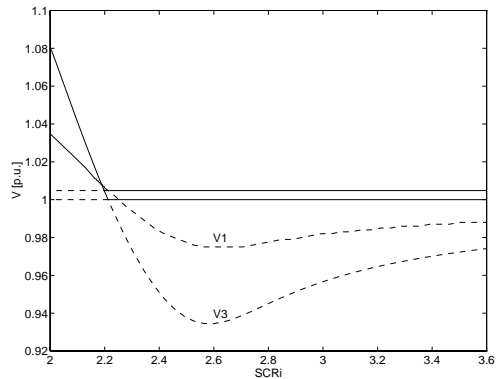


Fig. 2: Transcritical bifurcation diagram for ac converter voltages.

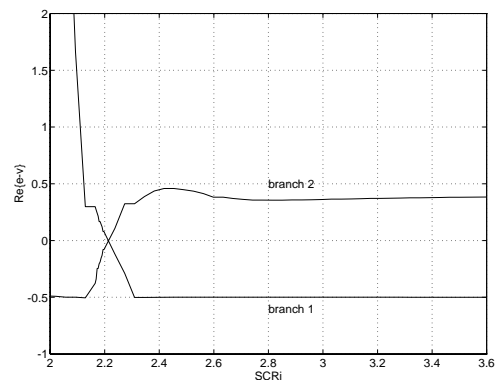


Fig. 3: Real part of the system eigenvalues closest to the imaginary axis on the complex plane for both branches of equilibria. The system presents a transcritical bifurcation at  $SCR=2.2123$ .

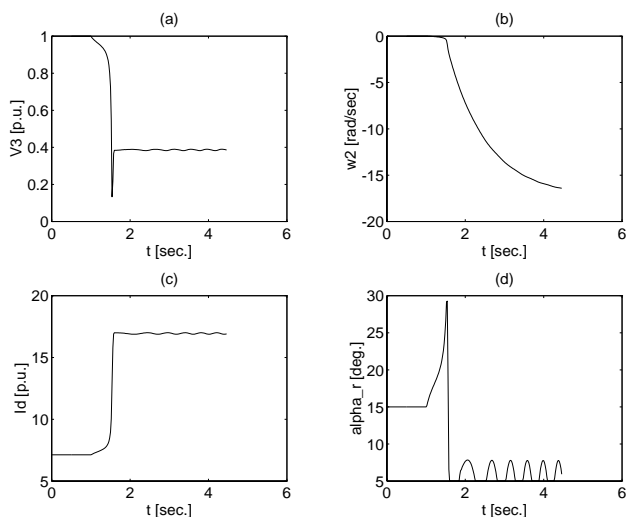
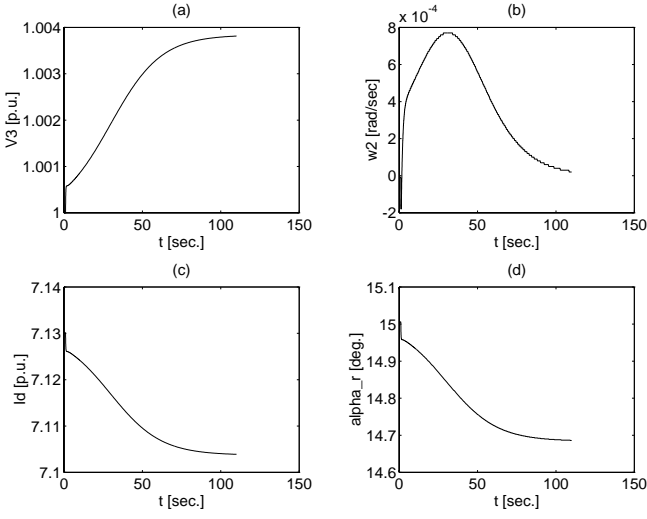


Fig. 4: Simulation of a SCR change from 2.24 to 2.20 at 1 sec., with a 0.5sec. delay on  $V_{t_{G_3}}$  change to maintain  $V_3$  at 1p.u. The (a) inverter ac voltage  $V_3$ , (b) generator  $G_3$  frequency  $\omega_3$ , (c) dc current  $I_d$ , and (d) rectifier firing angle  $\alpha_r$  are shown. The system is unstable.



**Fig. 5:** Simulation of a SCR change from 2.24 to 2.20 at 1 sec., with an instantaneous change on  $V_{tG_3}$  to maintain  $V_3$  at 1p.u. The (a) inverter ac voltage  $V_3$ , (b) generator  $G_3$  frequency  $\omega_3$ , (c) dc current  $I_d$ , and (d) rectifier firing angle  $\alpha_r$  are shown. The system recovers, approaching a new stable equilibrium point.

eigenvalues of the dynamic Jacobian  $D_x s_0$ . In this case, the eigenvalues of  $D_z \mathbf{F}|_0$  do not change in any significant way that would allow to determine the location of this bifurcation by using this matrix. The system matrices, i.e.,  $D_x s|_0$ ,  $D_z \mathbf{F}|_0$ , and the power flow Jacobian, do not become singular at the bifurcation point.

Two distinct direct methods can be used to find the exact position of the Hopf bifurcation point. The first method is based on a mathematical restatement of condition (9) [20, 29], thus, one has to solve

$$\begin{aligned} \mathbf{F}(\mathbf{x}, \mathbf{y}, \lambda) &= \mathbf{0} \\ D_x s|_0 \mathbf{v}_r &= -\beta \mathbf{v}_i \\ D_x s|_0 \mathbf{v}_i &= \beta \mathbf{v}_r \\ \|\mathbf{v}_r\| &\neq 0 \\ \|\mathbf{v}_i\| &\neq 0 \end{aligned} \quad (11)$$

where  $\mathbf{v}_r \pm j\mathbf{v}_i$  ( $\mathbf{v}_r, \mathbf{v}_i \in \mathbb{R}^n$ ) are the eigenvectors of the pair of complex conjugate eigenvalues  $\pm j\beta$ . The second method consists on solving equations (12) below, which can be easily obtained from equations (11) [20, 30],

$$\begin{aligned} \mathbf{F}(\mathbf{x}, \mathbf{y}, \lambda) &= \mathbf{0} \\ D_x s|_0^2 \mathbf{v} &= -\beta^2 \mathbf{v} \\ \|\mathbf{v}\| &\neq 0 \\ \mathbf{p}^T \mathbf{v} &= 0 \end{aligned} \quad (12)$$

where  $\mathbf{v} \in \text{Range}\{\mathbf{v}_r, \mathbf{v}_i\}$ , and  $\mathbf{p} \in \mathbb{R}^n$  is a known constant vector orthogonal to  $\mathbf{v}$ . Of these two methods, equations (11) present better sparsity characteristics but requires of  $n$  more equations than (12). In both cases, good initial conditions for all system variables and unknown vectors can be obtained from an equilibrium close to the bifurcation point, produced by the continuation method. Notice that in (12), a vector  $\mathbf{p} \notin \text{Range}\{\mathbf{v}_r, \mathbf{v}_i\}$  must be chosen, hence, good approximations of  $\mathbf{v}_r$  and  $\mathbf{v}_i$  are required. Unless an exact location of

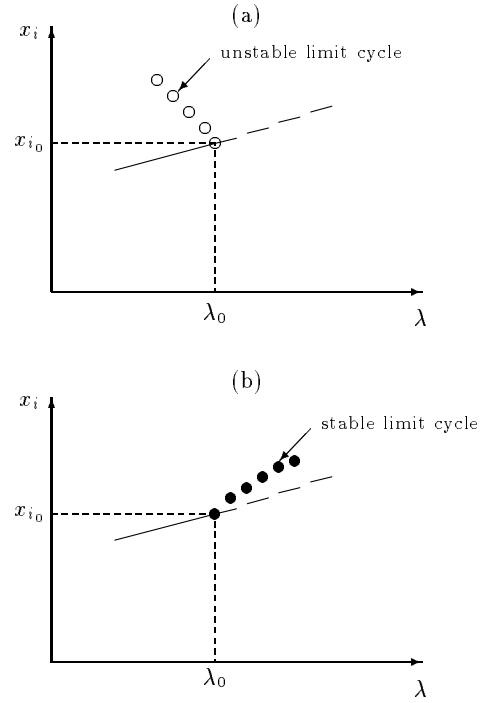


**Fig. 6:** Examples of (a) subcritical and (b) supercritical Hopf bifurcations. The symbols  $\circ$  and  $\bullet$  are used to depict half of the amplitude of the unstable and stable limit cycles, respectively.

the bifurcation point is needed, continuation methods usually suffice to determine the bifurcation. Furthermore, these direct methods are not useful in practice to locate Hopf bifurcations of systems represented by differential-algebraic equations (1), due to the computational difficulties of determining the symbolic Jacobian  $D_x s|_0$ . Although approximations to this Jacobian can be used, the convergence characteristics of the numerical methods used to solve equations (11) or (12) are significantly degraded.

Two types of Hopfs are possible depending on the stability of the limit cycle generated by the bifurcation, namely, subcritical and supercritical. Examples of these two types are depicted in Fig. 6 for a system modeled with equations (2). In this figure, the equilibrium points of a state variable  $x_i \in \mathbf{x}$  are depicted for several values of the parameter  $\lambda$ , and a Hopf bifurcation is shown at  $(\mathbf{x}_{i_0}, \lambda_0)$ . Half of the amplitude of the oscillation generated by the bifurcation is depicted using the symbols  $\circ$  (unstable) and  $\bullet$  (stable). For the subcritical bifurcation the corresponding limit cycle is unstable, whereas for the supercritical the limit cycle is stable [20].

The limit cycle generated by a Hopf bifurcation can be computed by solving the following Boundary Value Problem (BVP) for  $t \in [t_0, t_0 + T]$  [20]:

$$\begin{aligned} \begin{bmatrix} \dot{\mathbf{x}} \\ \dot{T} \end{bmatrix} &= \begin{bmatrix} \mathbf{s}(\mathbf{x}, \lambda) \\ 0 \end{bmatrix} \\ \text{s.t. } \mathbf{r}(\mathbf{x}(t_0), \mathbf{x}(t_0 + T)) &= \begin{bmatrix} \mathbf{x}(t_0) - \mathbf{x}(t_0 + T) \\ p(\mathbf{x}(t_0), \lambda) \end{bmatrix} = \mathbf{0} \end{aligned} \quad (13)$$

where  $p(\mathbf{x}(0), \lambda)$  is a phase condition to set the initial time  $t_0$ . This condition can be set to

$$p(\mathbf{x}(t_0), \lambda) = x_i(t_0) - k = 0$$

where  $x_i \in \mathbf{x}$ , and  $k \in \mathbb{R}^n$  is a fixed initial value of  $x_i(t)$  that must be in the desired solution range. Another possible phase condition is

$$p(\mathbf{x}(t_0), \lambda) = s_i(\mathbf{x}(t_0), \lambda) = 0$$

with  $s_i(\cdot) \in \mathbf{s}(\cdot)$ , so that the initial  $t_0$  is set to a local minimum or maximum of the oscillation of  $x_i(t)$ . The latter condition has the advantage of not requiring any previous knowledge of the solution range  $x_i(t)$  in  $t \in [t_0, t_0 + T]$ ; however,  $s_i(\cdot)$  should be linear in order to apply simple known methods to solve BVPs with linear boundary conditions  $\mathbf{r}(\mathbf{x}(t_0), \mathbf{x}(t_0+T))$  [31].

Normalizing the time interval to have a unit length, i.e.,  $t \in [0, 1]$ , BVP (13) becomes

$$\begin{aligned} \begin{bmatrix} \mathbf{x}' \\ T' \end{bmatrix} &= \begin{bmatrix} T \mathbf{s}(\mathbf{x}, \lambda) \\ 0 \end{bmatrix} \\ \text{s.t. } \mathbf{r}(\mathbf{x}(0), \mathbf{x}(1)) &= \begin{bmatrix} \mathbf{x}(0) - \mathbf{x}(1) \\ p(\mathbf{x}(0), \lambda) \end{bmatrix} = \mathbf{0} \end{aligned} \quad (14)$$

where  $\mathbf{x}'$  and  $T'$  denote the derivatives of  $\mathbf{x}$  and  $T$  w.r.t. the normalized variable  $t$ .

Current numerical techniques do not address the problem of solving differential-algebraic BVPs, and are limited in the number of states and equations that can efficiently handle. Moreover, due to the different nature of the BVPs that need to be solved, one has to use generic techniques proven to work in a variety of problems (e.g., the multiple shooting method [31]), rather than use more efficient methods which are model dependent (e.g., finite elements method [33]). Furthermore, BVP (14) introduces an additional zero equation that generates convergence problems if one does not start with a good initial guess for all system variables, particularly for the period  $T$ . An example to illustrate some of these problems is presented at the end of section 3.2.

Once the limit cycle is calculated for a given value of the parameter  $\lambda$ , one can proceed to address the issue of stability of these oscillations. The idea is simple, to determine the stability of a limit cycle one must answer the question of whether a system trajectory starting arbitrary close to the limit cycle converges to it (stable) or not (unstable). Hence, the distance between the system trajectory and the limit cycle at any point in time for a given  $\lambda$  can be defined as:

$$\| \mathbf{d}_\lambda(t) \| \triangleq \| \varphi_\lambda(t; \mathbf{x}(0) - \mathbf{d}_0) - \varphi_\lambda^T(t; \mathbf{x}(0)) \| \quad (15)$$

where  $\mathbf{x}(0)$  is the initial point of the oscillatory system trajectory  $\varphi_\lambda^T(t; \mathbf{x}(0))$  of period  $T$ , i.e.,

$$\mathbf{x}(0) = \mathbf{x}(T) = \varphi_\lambda^T(T; \mathbf{x}(0))$$

$\mathbf{d}_0$  is the initial distance between this limit cycle and the system trajectory  $\varphi_\lambda(t; \mathbf{x}(0) + \mathbf{d}_0)$  generated by the initial conditions  $\mathbf{x}(0) + \mathbf{d}_0$ . Then, the stability problem can be analyzed in two ways:

1. Use time simulations to solve an initial value problem with initial conditions  $\mathbf{x}(0) + \mathbf{d}_0$ , and see whether  $\| \mathbf{d}_\lambda(T) \| < \| \mathbf{d}_0 \|$  (stable limit cycle) or  $\| \mathbf{d}_\lambda(T) \| > \| \mathbf{d}_0 \|$  (unstable limit cycle). The limit cycle must be known beforehand, otherwise system trajectories that do not converge to it yield no information regarding the stability of the oscillations. The advantage of this method is that time simulations are relatively inexpensive.

Element	$G$	$B$	$-B_s$
Line 1-2	3.68	54.13	4.68
Line 2-3	3.68	54.13	4.68
Transf. $G_1$	0	166.67	0
Transf. $G_2$	0	100.00	0
Transf. $G_3$	0	100.00	0
Capac. 1	0	0	13.00
Capac. 3	0	0	13.68

**Table 4:** AC transmission system data in p.u. for a 550 kV and 100 MVA base.

Variable	$G_1$	$G_2$	$G_3$
Inertia $M$	0.1	0.016	$\infty$
Damping $D$	0.001	0.001	—
Terminal Voltage $V_t$	1	1	1
Mechanical Power $P_m$	40	4.75	—

**Table 5:** Generator data in p.u. for a 13.8 kV and 100 MVA base.

2. Determine the *monodromy matrix* [20], which is part of the first term on the Taylor series expansion around  $\mathbf{x}(0)$  of  $\mathbf{d}_\lambda(T)$  in (15), i.e.,

$$M_\lambda = \Phi_\lambda(T) = D_x \varphi_\lambda^T(T; \mathbf{x}(0)) \quad (16)$$

This matrix  $M_\lambda \in \mathbb{R}^{n \times n}$  has one eigenvalue  $\mu(M_\lambda) = 1$ . Hence, based on Floquet theory, one can show that if  $|\mu(M_\lambda)| < 1$  for all the remaining  $n - 1$  eigenvalues (Floquet multipliers), the associated limit cycle is stable, otherwise, if only one eigenvalue  $|\mu(M_\lambda)| > 1$ , the limit cycle is unstable. If more than one eigenvalue  $|\mu(M_\lambda)| = 1$ , then the limit cycle bifurcates leading the system to chaotic behavior. A more detailed discussion of the latter condition is carried out in section 4.

Calculation of the monodromy matrix (16) is a nontrivial task;  $M_\lambda$  can be approximated, however, by the product of several matrices generated during the numerical solution of BVP (14) with the multiple shooting method [20, 31].

### 3.2. Example

Tables 4, 5 and 6 show the steady state and dynamic data used in the system of Fig. 1 to generate a Hopf bifurcation. The SCR in the rectifier is 5.6, whereas the inverter side SCR is 3.3. The load at bus 2 is modeled as a frequency dependent active power plus a voltage dependent reactive power term, i.e.,

$$\begin{aligned} P_l &= P_{l_0} + dP + D_l \delta_2 \\ Q_l &= \left( \frac{V_2}{V_{2_0}} \right)^2 Q_{l_0} \end{aligned}$$

where  $P_{l_0} = 4.75$ ,  $Q_{l_0} = 1.561$ ,  $D_l = 0.1$ , and  $V_{2_0} = 1.01965$ , all in p.u. The active power load change at bus 2 is chosen as the slowly changing system parameter, i.e.,  $\lambda = dP$ ; thus, any local bifurcation associated to a zero eigenvalue is expected to be a saddle-node as discussed above. The infinite bus  $G_3$  absorbs all losses and load power changes in the system.

Figures 7 and 8 depict part of the bifurcation diagrams, PV or “nose” curves, obtained with the continuation method

Variable	Rectifier	Inverter
$K_P$	1	1
$K_I$	75	75
Commutation reactance $X_c$	0.1345	0.1257
Tap $a$	1.7634	1.7678
Min. firing angle $\alpha_{min}$	$5^\circ$	$\sim 120^{0\dagger}$
Max. firing angle $\alpha_{max}$	$120^\circ$	$\sim 142^{0\dagger}$
Min. extinction angle $\gamma_{min}$	$\sim 40^{0\dagger}$	$18^\circ$
Max. extinction angle $\gamma_{max}$	$\sim 155^{0\dagger}$	$40^\circ$
Current order $I_o$	1.0	0.9
Min. current order $I_{o_{min}}$ <sup>‡</sup>	0.1	0.0
Max. ac voltage $V_{ac_{max}}$ <sup>‡</sup>	0.95	0.95
Min. ac voltage $V_{ac_{min}}$ <sup>‡</sup>	0.5	0.5
DC resistance $R_d$	0.06236	
DC inductance $L_d$	0.01981	

<sup>†</sup> Assuming  $\mu \approx 20^0$     <sup>‡</sup> VDCOL

**Table 6:** DC system data in p.u. for a 550 kV and 2.5 kA base.

for the rectifier and inverter ac voltages when the parameter  $dP$  changes. These diagrams were traced up to the maximum value of  $dP$ , or maximum loading point, which corresponds to a saddle-node bifurcation at  $dP_{max} = 4466$  MW for the ac/dc system with no VDCOL (Fig. 7), and  $dP_{max} = 4683.6$  MW when VDCOL is included (Fig. 8). The continuous lines represent the s.e.p.s, whereas the dashed lines depict the u.e.p.s. Not all unstable equilibrium points were traced, since they are not relevant to this paper. Observe that in Fig. 7, the system is stable up to the saddle-node bifurcation, whereas in Fig. 8 the system loses stability due to a Hopf bifurcation before the saddle-node is encountered. Hence, from these results one can conclude that the VDCOL is the source of the Hopf bifurcation, but at the same time, this control mode increases the system loadability margin by about 5%, from  $dP_{max} = 4466$  MW to  $dP_{Hopf} = 4682.3$  MW. Although VDCOLs are typically designed to operate during transient conditions rather than in steady state, the VDCOL data used in this paper [32] enhances system stability by increasing the loadability margin.

The number of state variables in vector  $\mathbf{x}$  is  $n = 7$ , and the number of algebraic variables in  $\mathbf{y}$  is  $m = 10$ . By tracing the eigenvalues of the dynamic Jacobian  $D_x \mathbf{s}|_{0_{(7 \times 7)}}$  and the full system Jacobian  $D_z \mathbf{F}|_{0_{(17 \times 17)}}$  for all the equilibrium points depicted in Figs. 7 and 8, one can demonstrate that both become singular at the maximum loading point  $dP_{max}$ , as expected. However, the Hopf bifurcation depicted in Fig. 8 can only be detected by tracing the eigenvalues of  $D_x \mathbf{s}|_0$ , as explained above. Figure 9 depicts the behavior of the eigenvalues for the system equilibria around the Hopf and saddle-node bifurcations. Figures 9(a) and 9(b) show a complex pair of eigenvalues crossing the imaginary axis with non-zero speed before the saddle-node bifurcation, which is represented by the zero eigenvalue depicted in Figs. 9(a) and 9(c).

Direct methods (11) and (12) cannot be applied in practice to the ac/dc test system, due to the computational difficulties of determining the symbolic Jacobian  $D_x \mathbf{s}|_0$ . The continuation method and a trial and error approach was used here to successfully locate this bifurcation.

Figure 10 depicts the effect of the Hopf bifurcation in the ac/dc system. Observe the oscillations of all variables, partic-

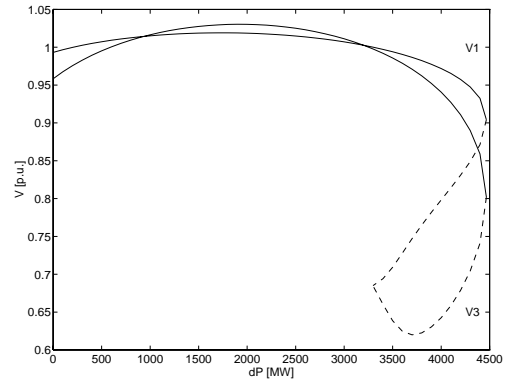


**Fig. 7:** Bifurcation diagram for ac/dc system with no VDCOL. There is a saddle-node bifurcation at  $dP_{max} = 4466$  MW.

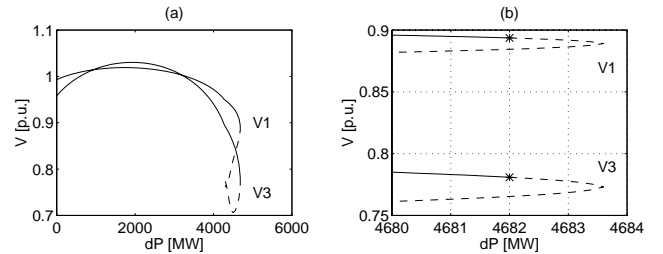


**Fig. 8:** Bifurcation diagrams for ac/dc system with VDCOL. Plot (b) depicts the region around  $dP = 4682.3$  MW where a Hopf bifurcation occurs before the saddle-node is encountered at  $dP_{max} = 4683.6$  MW.

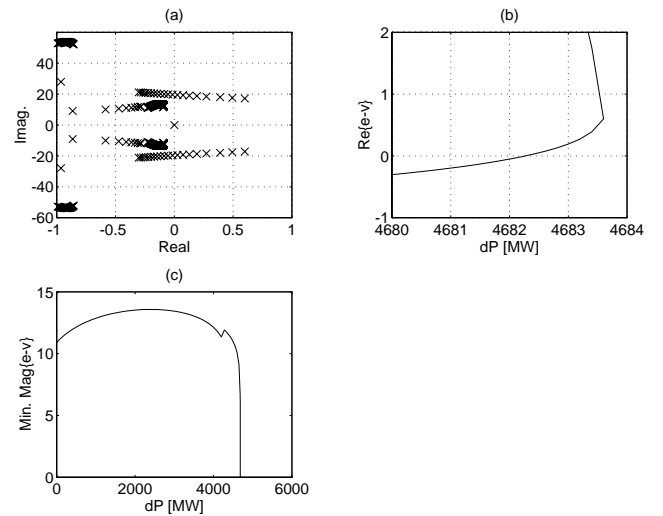


**Fig. 9:** Eigenvalues for ac/dc test system with VDCOL: (a) complex plane loci depicting a zero eigenvalue and the crossing of the imaginary axis of a pair of complex conjugate eigenvalues; (b) real part of complex eigenvalues closest to the imaginary axis showing the Hopf bifurcation at  $dP_{Hopf} = 4682.3$  MW; (c) minimum absolute magnitude depicting the saddle-node bifurcation at  $dP_{max} = 4683.6$  MW.

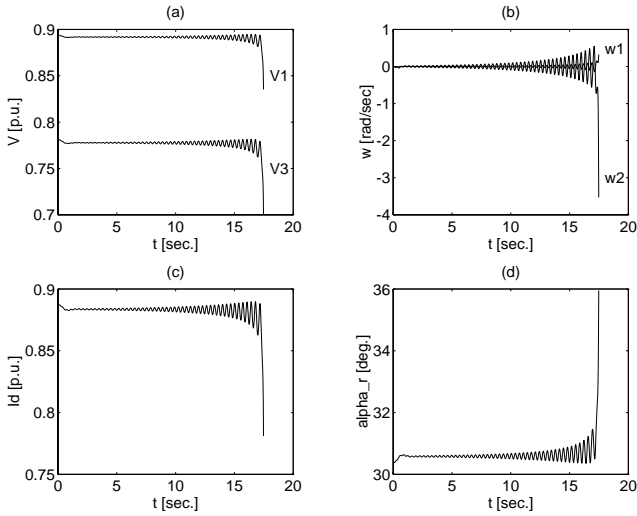


**Fig. 10:** Simulation of a change in  $dP$  from 4682 to 4683 MW at  $t = 0.1\text{sec}$ . The (a) rectifier  $V_1$  and inverter  $V_3$  voltages, (b) generators frequencies  $\omega_1$  and  $\omega_2$ , (c) dc current  $I_d$ , and (d) rectifier firing angle  $\alpha_r$  are shown. The system oscillates and becomes unstable.

ularly voltages and frequencies, before system collapse. From these simulations one cannot conclude whether the Hopf is subcritical or supercritical; for that type of analysis the limit cycles around the equilibria must be computed solving BVP (14), to then calculate the eigenvalues of the associated monodromy matrix, as previously explained. However, these types of studies could not be carried out on this example due to the limitations of the available numerical methods, simulation tools, and computer resources. To give the reader an idea of what is required to solve a BVP of the class represented by equations (14), a multiple shooting method with modified Newton-Raphson [31] was implemented in MATLAB to determine a stable limit cycle of a system of two state variables and no algebraic constraints. Depending on the initial guesses, this problem takes from 3-4 iterations to 15-20 iterations, with CPU times ranging from 10 minute to 3 hours in a dedicated 32MB-RAM SPARCSTATION-LX with a 50MHz MICROSPARC chip delivering a 21.0 SPECfp92. For an unstable limit cycle the method does not converge unless one starts from an initial guess very close to the final solution.

#### 4. Computational Requirements to Study Chaotic Behavior

A system modeled by a set of one-parameter differential equations can display chaotic behavior through several mechanisms, all based on a series of bifurcations of equations (2) [20]. As the system parameter  $\lambda$  changes, the limit cycles born of Hopf bifurcations also bifurcate. These types of bifurcations can be detected by monitoring the eigenvalues  $\mu(M_\lambda)$  of the monodromy matrix (16) for the various values of  $\lambda$ . Thus, the following bifurcations take place at  $\lambda = \lambda_0$  when one or two of the  $n - 1$  eigenvalues  $\mu(M_{\lambda_0})$  (one eigenvalue is always unity, say  $\mu_n(M_\lambda) = 1$ ) cross the unit circle in the complex plane [20]:

1. If  $\mu_j(M_{\lambda_0}) = 1$ , for some  $1 \leq j \leq n - 1$ , the limit cycle undergoes a saddle-node, transcritical or pitchfork bifurcation at  $\lambda_0$ . In this case, limit cycles appear or disappear and gain or lose stability, depending on the type of bifurcation. This phenomenon is similar to the bifurcations of equilibrium points, and can be associated to a singularity of the Jacobian of the related Poincaré map equations.
2. If  $\mu_j(M_{\lambda_0}) = -1$ , for some  $1 \leq j \leq n - 1$ , the limit cycle bifurcates through a period doubling bifurcation at  $\lambda_0$ . This bifurcation can be characterized by the emergence of a second limit cycle; hence, this bifurcation becomes apparent in the time domain by the system trajectories jumping alternatively from one limit cycle to another. An infinite series of period doublings lead the system to chaos. An example of this behavior in a simple power system model of 4 state variables and no algebraic constraints is shown in references [11, 34].
3. If a pair of complex conjugate eigenvalues  $\mu_j(M_{\lambda_0}) = \mu_k^*(M_{\lambda_0})$ , for some  $1 \leq j, k \leq n - 1$ , lie on the unit circle, i.e.,  $|\mu_j(M_{\lambda_0})| = |\mu_k(M_{\lambda_0})| = 1$ , the system presents a torus bifurcation or generalized Hopf bifurcation at  $\lambda_0$ . One can think of this bifurcation as the equivalent of the Hopf bifurcation in system equilibria. The torus bifurcation can be represented in the time domain as a torus like object, with system trajectories spiraling around it. Theoretical and experimental evidence point to a series of two consecutive torus bifurcations as another route to chaos.

To calculate the values of  $\lambda_0$  where these bifurcations take place for differential equations (2), and thus study the mechanisms that might lead to chaos, continuation and direct methods can be applied to the BVP (14). This problem can be reduced for both methods to solve BVPs of the form [20]

$$\begin{aligned} \begin{bmatrix} \mathbf{X}' \\ \lambda' \end{bmatrix} &= \begin{bmatrix} \mathbf{S}(\mathbf{X}, \lambda) \\ 0 \end{bmatrix} \\ \text{s.t.} \quad \begin{bmatrix} \mathbf{R}(\mathbf{X}(0), \mathbf{X}(1)) \\ \phi(\mathbf{X}(0)) \end{bmatrix} &= \mathbf{0} \end{aligned} \quad (17)$$

where  $\phi(\mathbf{X}(0))$  is a scalar and linear boundary condition required to compensate for the introduction of the constant  $\lambda$  as a system variable, and  $\mathbf{X}(t) \in \mathbb{R}^N$ ,  $t \in [0, 1]$ , represents the vector of the state variables  $\mathbf{x}$  and  $T$  in BVP (14) plus the new variables introduced to solve the desired problem, which vary with  $\mathbf{S}(\cdot)$  and  $\mathbf{R}(\cdot)$  according to the method used.

For example, to find the location of a period doubling bifurcation using the direct method, one should solve the following  $N = 2n + 3$  BVP:

$$\begin{aligned} \begin{bmatrix} \mathbf{x}' \\ T' \\ \lambda' \\ \mathbf{v}'_x \\ \mathbf{v}'_T \end{bmatrix} &= \begin{bmatrix} Ts(\mathbf{x}, \lambda) \\ 0 \\ 0 \\ TD_x s(\mathbf{x}, \lambda) \mathbf{v}_x + v_T s(\mathbf{x}, \lambda) \\ 0 \end{bmatrix} \\ \text{s.t.} \quad \begin{bmatrix} \mathbf{x}(0) - \mathbf{x}(1) \\ p(\mathbf{x}(0), \lambda) \\ \mathbf{v}_x(0) - \mathbf{v}_x(1) \\ \mathbf{v}_x^T \frac{\partial p}{\partial \mathbf{X}(0)}(\mathbf{x}(0), \lambda) \\ v_{x_k}(0) - 1 \end{bmatrix} &= \mathbf{0} \end{aligned} \quad (18)$$

BVP (18) comes from the linearization of the BVP (14) around the bifurcation point, i.e., for  $\tilde{s}(\cdot) \triangleq [s^T(\cdot) \ 0]^T$ ,  $\tilde{x} \triangleq [x^T \ T]^T$ , and  $\tilde{r}(\cdot) \triangleq [r^T(\cdot) \ p(\cdot)]^T$ , the linearization of (14) yields

$$\begin{aligned} \tilde{v}' &= D_{\tilde{x}}\tilde{s}(\tilde{x}, \lambda)\tilde{v} \\ \text{s.t. } A\tilde{v}(0) + B\tilde{v}(1) &= \mathbf{0} \end{aligned}$$

where

$$\begin{aligned} A &= D_{\tilde{x}(0)}\tilde{r}(\tilde{x}(0), \tilde{x}(1)) \\ B &= D_{\tilde{x}(1)}\tilde{r}(\tilde{x}(0), \tilde{x}(1)) \end{aligned}$$

$A$  and  $B$  are constant matrices for a linear set of boundary conditions  $\tilde{r}(\cdot)$ . Observe that  $\tilde{v} \triangleq [v_x^T \ v_T]^T$  could be viewed as the equivalent of the right eigenvector at a bifurcation of equilibrium points. These equations are similar to the ones used to find bifurcations of equilibria with direct methods.

Continuation methods for finding bifurcations of limit cycles is a two part process, similar to the continuation methods used to detect bifurcations in system equilibria. A predictor step is applied first to find an initial guess, which is then used in the corrector step to calculate the actual solution on the bifurcation branch. The corrector step requires the solution of an  $N = n + 2$  BVP similar to (17) for  $x$ ,  $T$ , and  $\lambda$ . On the other hand, the predictor step can be designed so that it uses by-products of the numerical solution of previous BVPs, particularly when multiple shooting methods are used [20]

Both continuation and direct methods need good initial guesses for convergence of the associated BVPs. Hence, this issue must be considered in the actual implementation of these methods.

For power systems represented by differential-algebraic equations (1), direct methods cannot be used in practice, since they require of  $D_x s(x, \lambda)$  or a good approximation of it. Continuation methods also present difficulties due to the need of having to solve a series of BVPs with algebraic constraints. Although available numerical techniques, particularly multiple shooting methods, can be modified to solve these problems, they will require of rather large computer resources, as previously discussed.

## 5. Conclusions

Transcritical and Hopf bifurcations in differential-algebraic power system models are thoroughly discussed in this paper. Examples of these bifurcations are illustrated in an realistic transient stability model of an ac/dc power system, showing their direct link to particular voltage control mechanisms in the system. The paper also shows the computational requirements for the study of these phenomena, and a new technique for tracing transcritical bifurcations diagrams is proposed, based on the generic characteristics of saddle-node bifurcations in power systems.

This paper demonstrates the need for implementing and modifying existing numerical techniques to solve differential-algebraic BVPs, especially for the study of the mechanisms that could lead a system to chaos. However, the large amount of computational resources required for these types of analyses, significantly limits the practical application of these techniques to realistic power system models. More research on the solution of large BVPs is required before the methods discussed in this paper can be used in real environments.

## REFERENCES

- [1] L. H. Fink, ed., *Proceedings: Bulk Power System Voltage Phenomena—Voltage Stability and Security*, ECC/NSF Workshop, Fairfax, VA, Ecc. Inc., August 1991.
- [2] Y. Mansour, ed., *Suggested Techniques for Voltage Stability Analysis*, IEEE/PES Report, 93TH0620-5PWR, 1993.
- [3] M. M. Begovic and A. G. Phadke, "Dynamic Simulation of Voltage Collapse," *IEEE Trans. Power Systems*, Vol. 5, No. 1, February 1990, pp. 198–203.
- [4] H. G. Kwatny, A. K. Pasrija, L. Y. Bahar, "Static Bifurcations in Electric Power Networks: Loss of Steady-State Stability and Voltage Collapse," *IEEE Trans. Circuits and Syst.*, Vol. 33, No. 10, October 1986, pp. 981–991.
- [5] I. Dobson and H. D. Chiang, "Towards a Theory of Voltage Collapse in Electric Power Systems," *Systems & Control Letters*, Vol. 13, 1989, pp. 253–262.
- [6] C. A. Cañizares, "On Bifurcations, Voltage Collapse and Load Modeling," presented at the IEEE/PES 1994 Summer Meeting for publication in the *IEEE Trans. Power Systems*.
- [7] C. A. Cañizares, F. L. Alvarado, C. L. DeMarco, I. Dobson, W. F. Long, "Point of Collapse Methods Applied to AC/DC Power Systems," *IEEE Trans. Power Systems*, Vol. 7, No. 2, May 1992, pp. 673–683.
- [8] B. Gao, G. K. Morrison, P. Kundur, "Voltage Stability Evaluation Using Modal Analysis," *IEEE Trans. Power Systems*, Vol. 7, No. 4, November 1992, pp. 1529–1542.
- [9] P. A. Löf, T. Smed, G. Anderson, D.J. Hill, "Fast Calculation of a Voltage Stability Index," *IEEE Trans. Power Systems*, Vol. 7, No. 1, February 1992, pp. 54–64.
- [10] J. Deuse and M. Stubbe, "Dynamic Simulation of Voltage Collapses," *IEEE Trans. Power Systems*, Vol. 8, No. 3, August 1993, pp. 894–904.
- [11] V. Ajjarapu and B. Lee, "Bifurcation Theory and its Application to Nonlinear Dynamical Phenomena in an Electrical Power System," *IEEE Trans. Power Systems*, Vol. 7, No. 2, February 1992, pp. 424–431.
- [12] E. H. Abed and P. P. Varaiya, "Nonlinear Oscillations in Power Systems," *International Journal of Electric Power & Energy Systems*, Vol. 6, 1984, pp. 37–43.
- [13] P. W. Sauer, B. C. Lesieutre, M. A. Pai, "Dynamic vs. Static Aspects of Voltage Problems," in [1], pp. 207–216.
- [14] T. J. Overbye and C. L. DeMarco, "Voltage Security Enhancement Using Energy Based Sensitivities," *IEEE Trans. Power Systems*, Vol. 6, No. 3, August 1991, pp. 1196–1202.
- [15] C. C. Liu and K. T. Vu, "Types of Voltage Collapse," in [1], pp. 133–141.
- [16] I. Dobson and L. Lu, "Voltage Collapse Precipitated by the Immediate Change in Stability When Generator Reactive Power Limits are Encountered," *IEEE Trans. Circuits and Syst.-I*, Vol. 39, No. 9, September 1992, pp. 762–766.
- [17] G. K. Morrison, B. Gao, P. Kundur, "Voltage Stability Analysis Using Static and Dynamic Approaches," *IEEE Trans. Power Systems*, Vol. 8, No. 3, August 1993, pp. 1159–1171.
- [18] C. A. Cañizares and F. L. Alvarado, "Point of Collapse and Continuation Methods for Large AC/DC Systems," *IEEE Trans. Power Systems*, Vol. 8, No. 1, February 1993, pp. 1–8.
- [19] J. Guckenheimer and P. Holmes, *Nonlinear Oscillations, Dynamical Systems, and Bifurcations of Vector Fields*, Springer-Verlag, New York, 1986.
- [20] R. Seydel, *From Equilibrium to Chaos—Practical Bifurcation and Stability Analysis*, Elsevier Science Publishers, North-Holland, 1988.

- [21] C. A. Cañizares, "Conditions for saddle-node bifurcations in AC/DC power Systems," accepted for publication in the *Int. J. of Electric Power & Energy Systems*, May 1994.
- [22] C. L. DeMarco and A. R. Bergen, "Application of Singular Perturbation Techniques to Power System Transient Stability Analysis," *Proc. ISCAS*, May 1984, pp. 597–601.
- [23] C. A. Cañizares, "Saddle-Node Bifurcations in Power Systems," *Proc. JIEE*, Quito, Ecuador, July 1993, pp. 222–229.
- [24] F. L. Alvarado, *Solver-Q*, Software Development and Distribution Center, University of Wisconsin-Madison, 1987.
- [25] S. A. Klein and F. L. Alvarado, *Engineering Equation Solver*, F-Chart Software, Middleton, Wisconsin, 1993.
- [26] *MATLAB*, The Math Works Inc., Natick, Massachusetts, 1993.
- [27] B. W. Char et al, *Maple V Language Reference Manual*, Springer-Verlag, 1991.
- [28] H. D. Chiang and F. F. Wu, "Stability of Nonlinear Systems Described by a Second-Order Vector Differential Equation," *IEEE Trans. Circuits and Systems*, Vol. 35, No. 6, June 1988, pp. 703–711.
- [29] F. L. Alvarado, "Bifurcations in Nonlinear Systems: Computational Issues," *Proceedings of ISCAS*, May 1990, pp. 922–925.
- [30] D. Roose, "An Algorithm for the Computation of Hopf Bifurcation Points in Comparison with other Methods," *Journal of Computational and Applied Mathematics 12 & 13*, North-Holland, 1985, pp. 517–529.
- [31] J. Stoer and R. Bilirsch, *Introduction to Numerical Analysis*, Springer-Verlag, 1980.
- [32] *Methodology of Integration of HVDC Links in Large AC Systems—Phase 1: Reference Manual*, EPRI EL-3004, March 1983.
- [33] W. Kaplan, *Advanced Mathematics for Engineers*, Addison Wesley, 1981.
- [34] H. D. Chiang, C. W. Liu, P. P. Varaiya, F. F. Wu, M. G. Lauby, "Chaos in a Simple Power System," *IEEE Trans. Power Systems*, Vol. 8, No. 4, November 1993, pp. 1407–1417.

**Claudio A. Cañizares** was born in Mexico, D.F. in 1960. In April 1984, he received the Electrical Engineer diploma from the Escuela Politécnica Nacional (EPN), Quito-Ecuador, where he was a Professor for several years. His MS (1988) and PhD (1991) degrees in Electrical Engineering are from the University of Wisconsin-Madison. Dr. Cañizares is currently an Assistant Professor at the University of Waterloo, Department of Electrical & Computer Engineering, and his research activities are mostly concentrated in the analysis of stability issues in ac/dc systems.

**Steve Hranilovic** is a second year student of the Department of Electrical & Computer Engineering at the University of Waterloo, where he is currently pursuing a BAsC degree in Electrical Engineering. Mr. Hranilovic has worked as an Undergraduate Research Assistant at the University of Waterloo and a Coop-student in several industries in Canada.